EDUCATUM JSMT Volume 11 Number 1 (2024)
ISSN 2289-7070 / e-ISSN 2462-2451(88-100)
https://ejournal.upsi.edu.my/index.php/EJSMT/index

Incorporation of Graphene Oxide/Metal Oxide into Modified Polyvinylidene Fluoride Membrane for the Degradation of Methylene Blue Dye through Adsorption-Photocatalytic Activity

Siti Nor Aisyah Jamilon[1,2], Suriani Abu Bakar[1,2*], Azmi Mohamed[1,3], Muqoyyanah[1,4], Rosmanisah Mohamat[1,2] and Ye Zar Ni Htwe[1,2]

[1] Nanotechnology Research Centre, Faculty of Science and Mathematics, Universiti Pendidikan Sultan Idris, 35900 Tanjung Malim, Perak, Malaysia
[2] Department of Physics, Faculty of Science and Mathematics, Universiti Pendidikan Sultan Idris, 35900 Tanjung Malim, Perak, Malaysia
[3] Department of Chemistry, Faculty of Science and Mathematics, Universiti Pendidikan Sultan Idris, 35900 Tanjung Malim, Perak, Malaysia
[4] Research Center for Advanced Materials, National Research and Innovation Agency (BRIN), 15314 South Tangerang, Banten, Indonesia

**Corresponding author*: suriani@fsmt.upsi.edu.my

Published: 11 February 2024

To cite this article (APA): Siti Nor Aisyah, J., Suriani, A. B., Azmi, M., Muqoyyanah, Rosmanisah, M., & Htwe, Y. Z. N. (2024). Incorporation of Graphene Oxide/Metal Oxide into Modified Polyvinylidene Fluoride Membrane for the Degradation of Methylene Blue Dye through Adsorption-Photocatalytic Activity. *EDUCATUM Journal of Science, Mathematics and Technology*, *11*(1), 88–100. https://doi.org/10.37134/ejsmt.vol11.1.9.2024

To link to this article: https://doi.org/10.37134/ejsmt.vol11.1.9.2024

Abstract

Recent studies have demonstrated substantial advancements in the treatment of dye wastewater through the synergistic incorporation of graphene oxide (GO) and metal oxide. This research focuses on the successful fabrication of a GO-based composite membrane using the non-solvent induced phase separation (NIPS) method. Two distinct metal oxides, titanium dioxide (TiO_2) and zinc oxide (ZnO), were incorporated into polyvinylidene fluoride (PVDF) as the membrane carrier. The resulting membranes, namely PVDF/TiO2, PVDF/ZnO, and PVDF/TiO2/GO, were developed as photocatalyst membranes for the treatment of methylene blue (MB) dye contamination through adsorption-photocatalytic activity. The adsorption process was conducted for 30 minutes before initiating the photocatalytic activity. Upon UV-Vis measurement, the PVDF/TiO_2/GO composite membrane exhibited superior dye degradation efficiency, reaching 91.89%, as compared to PVDF/TiO_2 (91.38%) and PVDF/ZnO membrane (86.80%). This noteworthy enhancement in dye degradation performance, positions the PVDF/TiO2/GO composite membrane as a promising candidate for applications as a photocatalyst in the treatment of dye wastewater. The results underscore the potential effectiveness of this composite membrane in addressing environmental challenges associated with dye pollution.
Keywords: Adsorption-photocatalysis; Graphene Oxide; Titanium Dioxide; Zinc Oxide; Polyvinylidene Fluoride; Photocatalyst

INTRODUCTION

The development of the textile industry leads a significant contribution to worldwide economic expansion and encounters a critical environmental predicament in the form of wastewater that contains a diverse range of dyes [1]. The growing demand for textiles requires the use of modern water treatment techniques to remove colour pollutants efficiently. The dye wastewater can be tackled by combining an adsorption and photocatalysis process. The utilisation of the adsorption-photocatalysis technique has several advantages

including reduced time requirements, prolonged lifespan of the adsorbent, and improved efficiency [2]. This method involves the capture of pollutants through adsorption, followed by the utilisation of photocatalysis to generate reactive oxygen species (ROS) for the degradation of pollutants [3].

In the context of wastewater treatment, enhancing the capabilities of treatment processes can be achieved by modifying polymeric membranes, specifically those crafted from polyvinylidene fluoride (PVDF) [4]–[6]. The fabrication of photocatalyst membranes involves integrating inorganic and polymeric components using techniques like dip-coating, self-assembly, layer-by-layer deposition, and phase inversion [7]. Particularly, the non-solvent induced phase separation (NIPS) as a phase version has gained attention due to its cost effectiveness, simplicity, and equipment efficiency [8], [9]. NIPS ensures a uniform distribution of photocatalysts within the membrane, enhancing photocatalytic efficiency. Although NIPS is well-explored in membrane filtration, its application in membranes as adsorbents and photocatalysts remains an area requiring further exploration [10].

Moreover, the utilisation of PVDF membranes has been extensively observed in diverse filtration procedures owing to their notable chemical resistance and long-lasting nature [11]. Nevertheless, the traditional application of these membranes in the treatment of textile wastewater has challenges in attaining an integrated approach for adsorption-photocatalytic degradation. In order to tackle this particular difficulty, the current study emphasises the incorporation of novel nanomaterials, namely graphene oxide (GO) with metal oxides titanium dioxide (TiO_2) and zinc oxide (ZnO) into PVDF membranes. The objective of this integration is to improve the efficiency of the membrane, specifically in relation to the distinctive wastewater composition found in the textile sector. Table 1 shows a comparison of the photodegradation efficiency with different photocatalyst materials.

According to the results reported by Sheshmani and Nayebi, [12], the incorporation of GO demonstrated a reduction of TiO_2 bandgap value from 3.2 eV (pure TiO_2) to 3.0 eV (GO/TiO_2). Significant decreased of GO/TiO_2 charge carriers recombination rate further resulted in the better photodegradation efficiency up to 99.99% as compared to pure TiO_2 (30%). This result was in a good agreement with other study where incorporation of GO with TiO_2 demonstrated higher photodegradation efficiency (93%) compared to pure TiO_2 (80%) [13]. Puneetha et al., [14] reported that ZnO bandgap value was successfully reduced from 2.81 eV (pure ZnO) to 2.71 eV with the GO presence in the ZnO-based hybrid sample. The smaller band gap of the ZnO/GO hybrid futher contributes to its heightened photocatalytic activity with an efficiency of up to 99%, surpassing the 82% efficiency of pure ZnO. Meanwhile, Fischer et al., [15] reported the hydrophilic TiO_2/PVDF membrane showed the highest photocatalytic activity (100%) compared to hydrophilic TiO_2/PES membrane (70%).

Table 1. presents a comparison of the photodegradation efficiency with different photocatalyst materials

Material	Dye	Photodegradation efficiency	References
GO/TiO_2 nanocomposite	Remazol Black B (RBB)	99.9%	[12]
Cellulose/GO/TiO_2	Methylene Blue (MB)	93%	[13]
ZnO/GO	Crystal Violet (CV)	99%	[14]
PVDF/TiO_2	MB	100%	[15]

In this work, the novel combination of GO and metal oxide (TiO_2 and ZnO) with PVDF as polymer carrier using the NIPS method were successfully fabricated. Afterward, these fabricated membranes were employed for MB dye degradation to study their performance. To the best of our knowledge, the novelty of this study lies on the GO, TiO_2 and ZnO hybridisation with PVDF for adsorption-photocatalysis application. Furthermore, The PVDF hybrid photocatalyst membrane with GO, TiO_2 and ZnO presence for adsorption-photocatalysis application are not well explored. We believe that this work is the first attempt to evaluate the relative competitiveness of PVDF/TiO_2, PVDF/ZnO and PVDF/TiO_2/GO membranes as photocatalysts in adsorption-photocatalysis process.

MATERIALS AND METHODS

Materials

PVDF, specifically Kynar 760 in palette form, served as the polymer carrier in this study. Commercially sourced TiO_2 with a purity of ⩾99.5% (Sigma-Aldrich) and ZnO nanoparticles, also with a purity of ⩾ 99.5% (Sigma-Aldrich), were employed as additives.The synthesis of GO involved the use of commercial single-tail sodium dodecyl sulfate (SDS) surfactant, graphite rods measuring 150 mm in length and 10 mm in diameter (Goodfellow GmbH, Germany, 99.99% purity) as electrodes, and N, N-dimethylacetamide (DMAc) as the solvent. For the adsorption-photocatalysis test, MB dye sourced from Sigma Aldrich was utilized.

Synthesis of GO and fabrication of nanocomposite membrane

The electrochemical exfoliation method, as previously documented in references [8], [11], [16], [17]. was employed for the synthesis of GO in this study. Subsequently, the fabrication of photocatalyst membranes was conducted through the NIPS method. For the preparation of PVDF/TiO_2 and PVDF/ZnO membrane solutions, a mixture comprising 82 wt% DMAc, 15 wt% PVDF, and 3 wt% TiO_2 or ZnO was meticulously formulated. Conversely, the solution for the PVDF/TiO_2/GO membrane involved blending 15 wt% PVDF and 3 wt% TiO_2 with an 82 wt% DMAc_GO solution. Subsequent to their formulation, the membrane solutions (PVDF/TiO_2, PVDF/ZnO, and PVDF/TiO_2/GO) underwent a 24-hour stirring process at 70°C to achieve homogeneity. Post-stirring, these homogeneous solutions were left at room temperature overnight to eliminate any entrapped air bubbles. To produce the membranes, the homogenous solutions were casted using a casting knife on a glass plate with a precise 200 µm casting gap. Finally, the casted membranes were directly immersed in deionized water (DI) and stored for subsequent utilization. This meticulous procedural approach ensured the generation of well-prepared and bubble-free membranes suitable for further scientific experimentation.

Characterisation

The membrane surface and cross-sectional morphology were subjected to comprehensive characterization using a Field Emission Scanning Electron Microscopy (FESEM) instrument, specifically the Hitachi SU8020 model. To facilitate optimal cross-sectional observations, a 2 x 2 cm^2 membrane sample underwent a controlled fracture induced by liquid nitrogen immersion prior to FESEM analysis. Subsequently, a thin gold layer coating was applied to the membrane samples to enhance surface conductivity for precise analysis. Elemental compositions of the samples were determined through Energy Dispersive X-ray Analysis (EDX) using the Horiba EMAX instrument. For studying structural properties, Micro-Raman spectroscopy was employed, utilizing the Renisha InVia microRaman System. Furthermore, Fourier Transform Infrared (FT-IR) spectroscopy, conducted with a Perkin Elmer instrument, was employed to elucidate the functional groups present in the fabricated membranes. The FT-IR analysis spanned the region of 400-4000 cm^{-1} and incorporated an Attenuated Total Reflection (ATR) accessory. Concurrently, the crystalline properties of the membrane samples were assessed using X-ray Diffraction (XRD) via the Rigaku-Miniflex 600 instrument. The diffraction patterns of the fabricated membranes were obtained using Cu Kα radiation in the 2θ range from 5° to 80° at a rate of 1/min (40 kV, 40 mA, λ=1.54060). This comprehensive suite of analytical techniques provided a nuanced and detailed characterization of the membrane's physical, elemental, and structural attributes, contributing to a deeper understanding of its properties.

Photocatalytic degradation of MB

The membrane sample, possessing a surface area of 7 x 7 cm^2, was introduced into a container containing a 10 ppm concentration of MB dye solution. Subsequently, the samples underwent an adsorption process for a predetermined duration before the commencement of photocatalytic activity. Upon reaching adsorption-desorption equilibrium, the MB dye solution and membrane samples were subjected to

irradiation with a UV lamp emitting at a wavelength of 365 nm for a duration of 24 hours. Samples were extracted at hourly intervals and analyzed using Ultraviolet-Visible (UV-Vis) spectroscopy (Agilent Cary 60) within the wavelength range of 200 to 800 nm.

The photodegradation efficiency (η) was calculated using Equation 1:

$$\eta\ (\%) = \frac{(C_o - C_{eq})}{C_o} \times 100\%$$

Where C_o (ppm) and C_{eq} (ppm) are the initial and final of MB concentration, respectively. This rigorous experimental procedure allowed for the precise determination of the photodegradation efficiency of the membrane in the context of methylene blue dye degradation.

RESULTS AND DISCUSSION

FESEM and EDX analysis

The examination of different photocatalyst membranes involved a detailed analysis of the surface morphology and cross-section using FESEM. In Figure 1, the surface morphology, cross-section view, and EDX spectra of the fabricated PVDF/TiO_2 photocatalyst membranes are depicted. The smooth surface of PVDF/TiO_2 membranes without cracks, as observed in Figure 1 (a), indicates a well-dispersed additive within the membrane matrix. The presence of TiO_2 particles (indicated by yellow arrows) and PVDF (indicated by orange arrows) throughout the PVDF/TiO_2 membrane signifies the successful blending of the TiO_2 additive into the PVDF membrane components. This observation corroborates the findings of Benhabiles et al., [18], providing further evidence of successful additive integration into the PVDF membrane matrix.

Figure 1 (b) illustrates the cross-section of the PVDF/TiO_2 membrane, revealing a thin and dense skin layer with a finger-like structure and a thicker spongy structure at the bottom layer. The membrane exhibits a pore size ranging from 4.56 to 8.73 μm with a thickness of 69.0 μm. The larger pore size enhances the adsorption of molecules on the PVDF/TiO_2 membrane, and the larger pores allow for more extensive light penetration, influencing the dispersion of the photocatalytic reaction [19].

The elemental composition of PVDF/TiO_2 membranes was confirmed through EDX analysis, as depicted in Figure 1 (c). The higher and lower atomic percentages of F (51.68%) and Ti (3.79%), respectively, were detected. Additionally, the atomic percentages of 5.57 and 38.95% further confirmed the presence of O and C in the PVDF/TiO_2 membrane as well as completing the comprehensive understanding of its elemental composition.

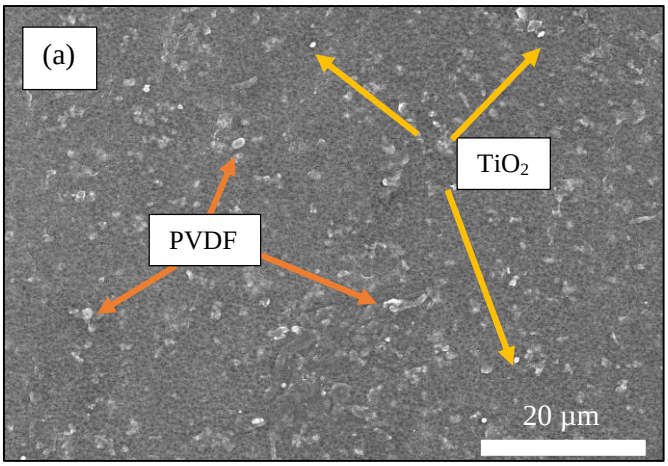

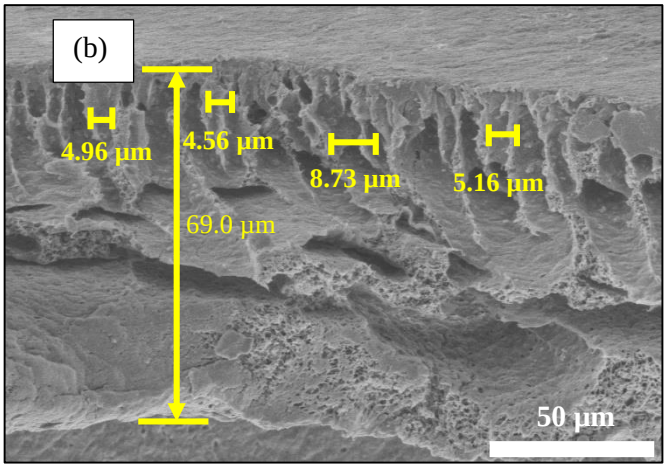

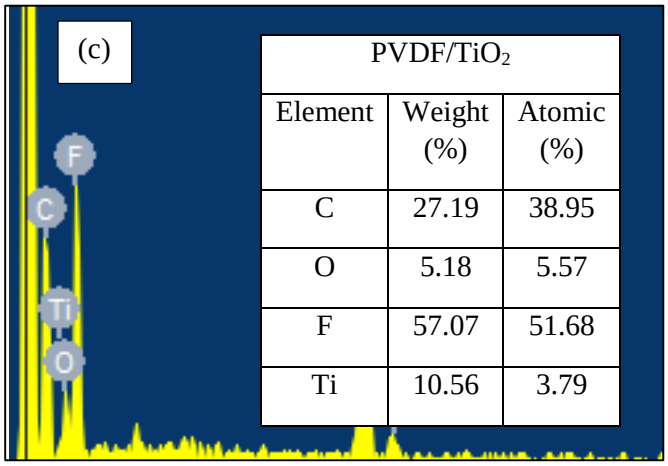

PVDF/TiO_2		
Element	Weight (%)	Atomic (%)
C	27.19	38.95
O	5.18	5.57
F	57.07	51.68
Ti	10.56	3.79

Figure 1. illustrates the FESEM image of; (a) surface morphology, (b) cross-section and (c) EDX spectra of the fabricated PVDF/TiO_2 photocatalyst membrane

Figure 2 presents a comprehensive characterization of the fabricated PVDF/TiO_2 photocatalyst membranes, encompassing surface morphology, cross-sectional analysis, and an elemental composition assessment via Energy Dispersive X-ray (EDX) spectroscopy. In Figure 2(a), the PVDF/ZnO membrane manifests a notably smooth surface, wherein the red arrows denote the presence of ZnO, while the orange arrows indicate PVDF. The ensuing cross-sectional perspective in Figure 2(b) reveals a similarity between the PVDF/ZnO and PVDF/TiO_2 membranes, albeit with discernible differences. Specifically, the pore sizes in the PVDF/ZnO membrane, ranging from 4.46 to 7 µm, are comparatively smaller than those in the PVDF/TiO_2 membrane. This variance arises from the heightened interaction between ZnO nanoparticles and PVDF, resulting in the formation of smaller pores during phase separation [20].

Further examination of the membranes indicates a slightly increased thickness in the PVDF/ZnO membrane (69.2 µm) in contrast to the PVDF/TiO2 membrane (69.0 µm). This discrepancy may be attributed to the disparate densities and mechanical properties of TiO2 and ZnO. Notably, the PVDF/ZnO membrane tends to form denser structures due to diminished material density and augmented mechanical strength [21]. The packing density of particles in the PVDF/ZnO membrane is less, potentially generating greater internal forces.

The EDX analysis conducted on the PVDF/ZnO membrane, as depicted in Figure 2(c), furnishes valuable insights into the elemental composition. Notably, the atomic percentage of carbon (C) is prominent at 54.85%, followed by oxygen (O) at 36.34%. Zn, representing the ZnO component, constitutes a lower atomic percentage of 4.22%. This elemental distribution underscores the unique composition of the PVDF/ZnO membrane, highlighting its potential implications for photocatalytic applications.

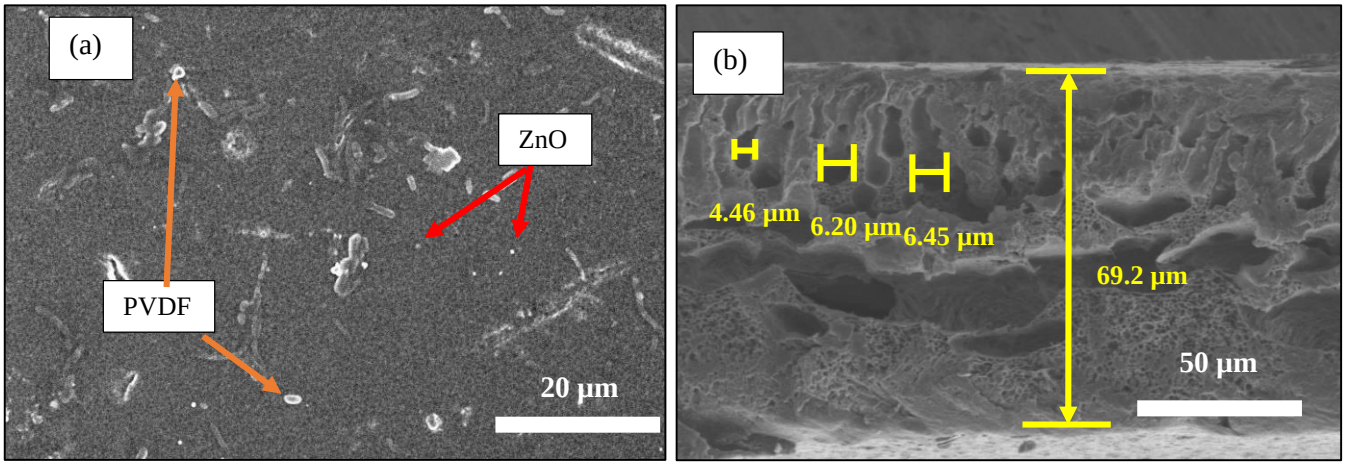

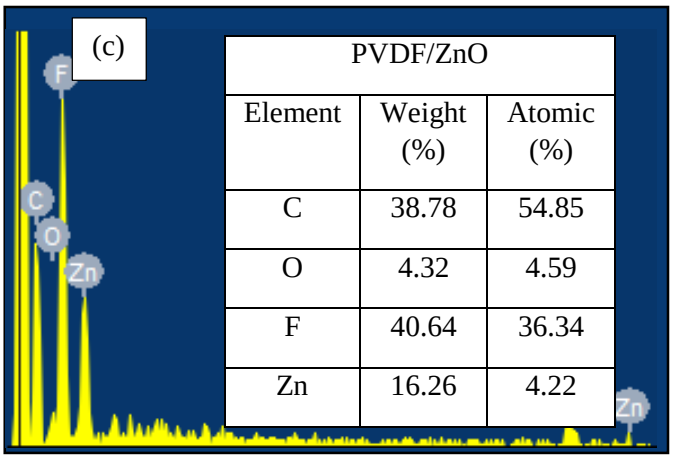

PVDF/ZnO		
Element	Weight (%)	Atomic (%)
C	38.78	54.85
O	4.32	4.59
F	40.64	36.34
Zn	16.26	4.22

Figure 2. FESEM image of; (a) surface morphology, (b) cross-section and (c) EDX spectra of the fabricated PVDF/ZnO photocatalyst membrane

In Figure 3(a), the surface of the PVDF/TiO_2/GO membrane exhibits a distinct smoothness, indicative of the successful integration of the GO layer, as denoted by the green arrows. Concurrently, the yellow arrows highlight the dispersion of TiO_2 particles within the membrane, confirming the presence of both components in the composite structure. Notably, the PVDF/TiO_2/GO membrane demonstrates an elongated finger-like structure with larger pore sizes ranging from 5.36 to 10.7 µm, surpassing those observed in the PVDF/TiO_2 and PVDF/ZnO membranes (Figure 3(b)). Furthermore, the PVDF/TiO_2/GO membrane boasts a marginally increased thickness of 69.8 µm compared to its counterparts. This augmentation is attributed to the accelerated solvent and non-solvent exchange rates facilitated by the presence of GO during the phase inversion process [17].

The enlarged pore size in the PVDF/TiO_2/GO membrane enhances molecular adsorption, while simultaneously facilitating improved light penetration. This feature holds significance in influencing the dispersion of photocatalytic reactions within the membrane. Meanwhile, the EDX analysis depicted in Figure 3(c) reveals an atomic percentage of carbon (C) at 46.52%, surpassing oxygen (O) at 20.00%, fluorine (F) at 30.73%, and titanium (Ti) at 2.75%. These findings affirm the presence of TiO_2 and GO nanoparticles on the surface of the PVDF membrane, substantiating the successful incorporation of these constituents into the composite structure.

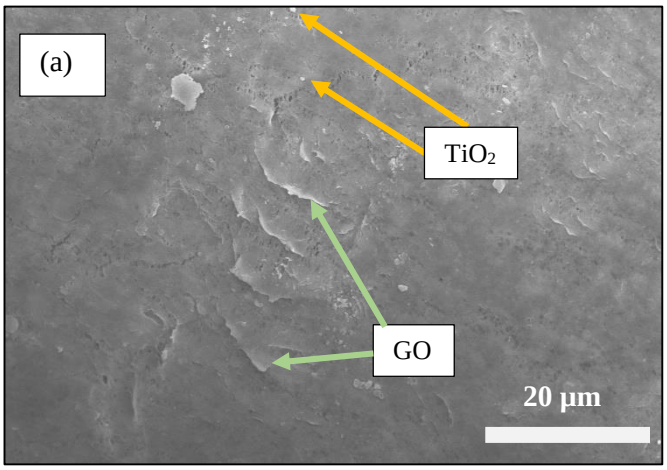

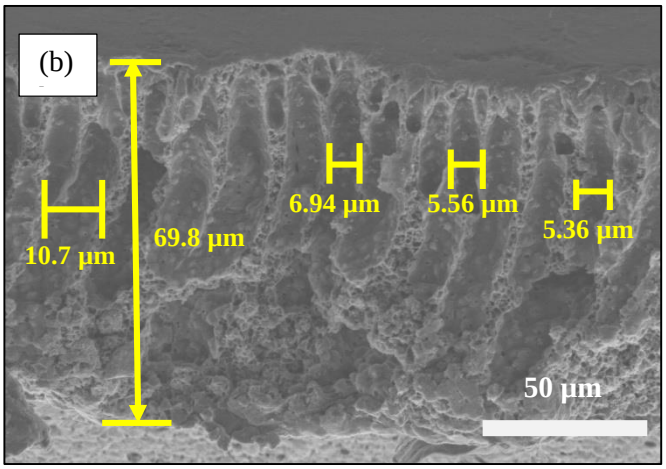

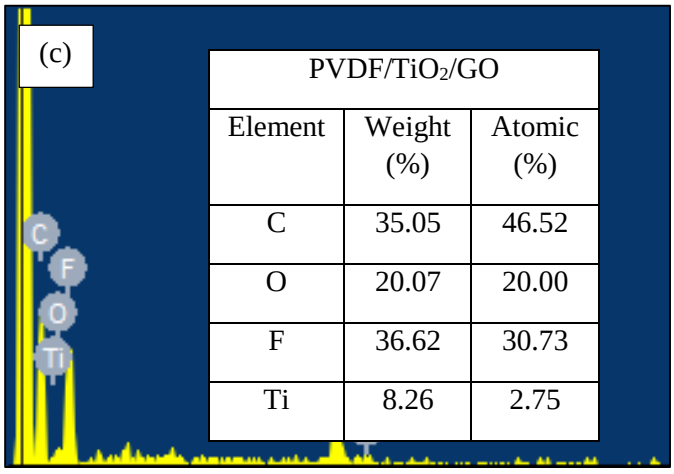

PVDF/TiO_2/GO		
Element	Weight (%)	Atomic (%)
C	35.05	46.52
O	20.07	20.00
F	36.62	30.73
Ti	8.26	2.75

Figure 3. presents the FESEM image of; (a) surface morphology, (b) cross-section and (c) EDX spectra of the fabricated PVDF/TiO_2/GO photocatalyst membrane

Micro-Raman analysis

Figure 4 displays the micro-Raman spectra of the PVDF-based nanocomposite photocatalyst membranes, providing insights into the presence and vibrational characteristics of GO, TiO_2, and ZnO. For the PVDF/TiO_2 membrane, a distinctive peak at 142.85 cm^{-1} is observed, corresponding to the E_g mode of the anatase phase of TiO_2. This mode signifies the symmetric stretching of the Ti-O bond in the lattice [22]. However, the absence of A_{1g}, B_{1g}, and B_{2g} peaks of the TiO_2 anatase phase indicates a modification in the nanoparticles' vibrational behaviour due to interactions with the PVDF matrix. Consequently, the identification of these peaks becomes challenging [23]. In the case of the PVDF/ZnO membrane, a discernible peak at 438.65 cm^{-1} is noted, corresponding to the E_2 (high) mode of ZnO. This peak is attributed to the vibration of oxygen atoms within the hexagonal plane [14].

The micro-Raman spectrum of the PVDF/TiO_2/GO membrane reveals a TiO_2 peak at 145.31 cm^{-1}, influenced by the presence of GO [23]. It is proposed that oxygen-containing functional groups of GO interact with the TiO_2 nanoparticles, influencing their vibrational characteristics [24], [25]. Next, the existence of GO in this sample was confirmed by the D- and G- band presence[16], [26], where the D-band (1331.46 cm^{-1}) represents defects in the graphite domain, and the G-band (1692.90 cm^{-1}) signifies the sp^2 hybridization of carbon atoms. The intensity ratio of D- and G-bands (I_D/I_G) is indicative of structural quality and disorder in carbon-based materials, with a higher I_D/I_G ratio suggesting a greater level of defects and disorder. The PVDF/TiO_2/GO membrane exhibits a higher I_D/I_G ratio of 1.62, confirming a high level of defects in GO during the exfoliation process and a greater number of oxygen-functional groups [11].

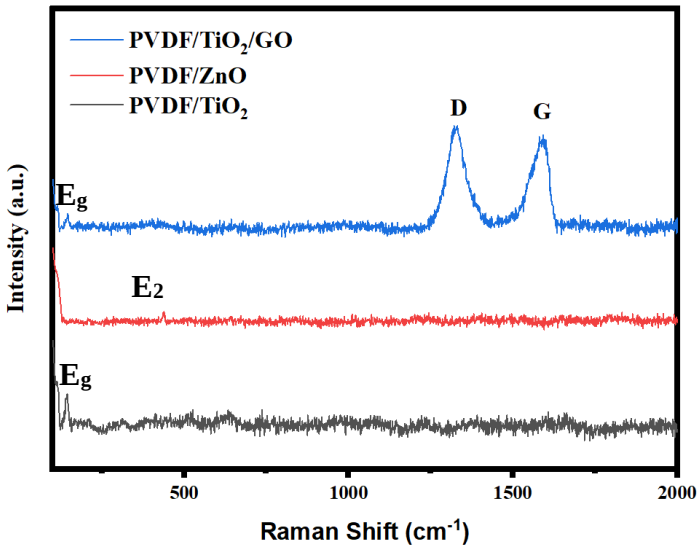

Figure 4. showcases the Micro-Raman spectroscopy of the fabricated PVDF-based nanocomposite photocatalyst membranes

FTIR analysis

FTIR analysis was employed to discern the chemical functional groups within the fabricated PVDF-based nanocomposite photocatalyst membrane. Figure 5 portrays the FTIR spectra, offering insights into the molecular composition of the membranes. In Figure 5(a), the α-phase of PVDF is delineated at 762 cm^{-1} for PVDF/TiO_2 and PVDF/ZnO membranes. Notably, the introduction of graphene oxide (GO) in the PVDF/TiO_2/GO membrane induces a slight shift of this peak to 760 cm^{-1} [27]. The β-phase of PVDF/TiO_2 and PVDF/ZnO membranes is identified at 840 cm^{-1}, 876 cm^{-1}, and 1274 cm^{-1}. The β-phase peaks in PVDF/ZnO membrane shift marginally to 840 cm^{-1}, 874 cm^{-1}, and 1276 cm^{-1}, possibly due to the physical interaction between PVDF and ZnO nanoparticles [4]. The presence of GO intensifies and sharpens the β-phase peaks in PVDF/TiO_2/GO membrane, evidenced by peaks at 836 cm^{-1}, 876 cm^{-1}, and 1274 cm^{-1} [27].

Additionally, a distinctive peak at 1402 cm^{-1} signifies C-H stretching vibration in PVDF/TiO_2 membrane, with a slight shift to 1400 cm^{-1} in PVDF/ZnO due to the synergistic effect between PVDF and ZnO nanoparticles [14]. In PVDF/TiO_2/GO membrane, the C-H bond is detected at 1400 cm^{-1}, indicating interactions between the molecular chains of PVDF and the diverse functional groups on the GO surface [28]. Confirmation of TiO_2 presence in PVDF/TiO_2 membrane is derived from peaks at 472 cm^{-1} and 1660 cm^{-1}, with a shift to 466 cm^{-1} and 1660 cm^{-1} in PVDF/TiO_2/GO membrane, possibly influenced by the presence of GO altering the composition and distribution of TiO2 [29]. ZnO presence in PVDF/ZnO membrane is validated by a peak at 482 cm^{-1}, representing the Zn-O bond [30]. Figure 5(b) reveals a broad peak in the range of 3256 - 3420 cm^{-1}, attributed to the -OH bond stretching vibration of GO in PVDF/TiO_2/GO membrane. This signifies the presence of oxygen-functional groups within the membrane [17].

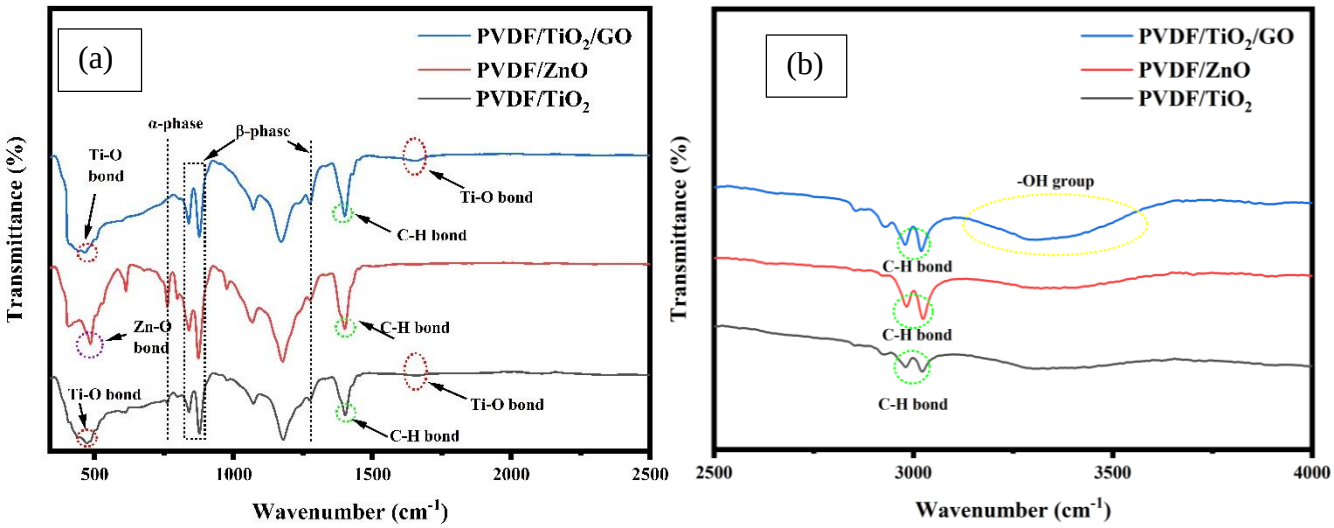

Figure 5. illustrates both (a) FTIR spectra and (b) the GO peaks enlargement of the fabricated PVDF-based nanocomposite photocatalyst membranes

XRD analysis

The XRD (X-ray Diffraction) analysis depicted in Figure 6 provides a comprehensive insight into the structural characteristics of the fabricated PVDF-based nanocomposite photocatalyst membranes.
In the case of PVDF/TiO_2, the α-phase crystallinity is affirmed by discernible diffraction peaks at 18.38° and 20.35°. Additional peaks at 25.30°, 27.43°, 37.81°, 48.01°, 53.95°, 55.06°, and 62.67° signify the presence of the anatase phase of TiO_2 within the membrane [13], [29]. Moving to PVDF/ZnO, the α-phase crystallinity manifests at diffraction peaks of 18.42° and 20.08°. Furthermore, distinctive peaks at 31.87°, 54.53°, 36.35°, 47.63°, 56.69°, 62.95°, and 68.03° confirm the presence of ZnO in the PVDF/ZnO membrane [31].

For PVDF/TiO_2/GO membrane, the α-phase crystallinity of PVDF for PVDF/TiO_2/GO membrane was slightly shifted to 20.64°. This situation was believed due to the GO presence in polymer matrix [29]. In addition, the TiO_2 peak of PVDF/TiO_2/GO membrane were slightly shifted to 25.34, 27.54, 37.85, 48.07, 54.01, 55.23 and 62.82° compared to PVDF/TiO_2 membrane, which might be due to the interaction between TiO_2 and GO [32]. It is noteworthy that GO is not distinctly identified in the XRD spectra of PVDF/TiO_2/GO, possibly due to its lower loading amount and interactions with TiO_2 that disrupt the stacked sheets of GO. This phenomenon emphasizes the intricacies of the interactions within the composite structure, particularly between TiO_2 and GO [11], [16]. The XRD analysis thus unravels the nuanced crystalline characteristics and interactions present in the PVDF-based nanocomposite photocatalyst membranes.

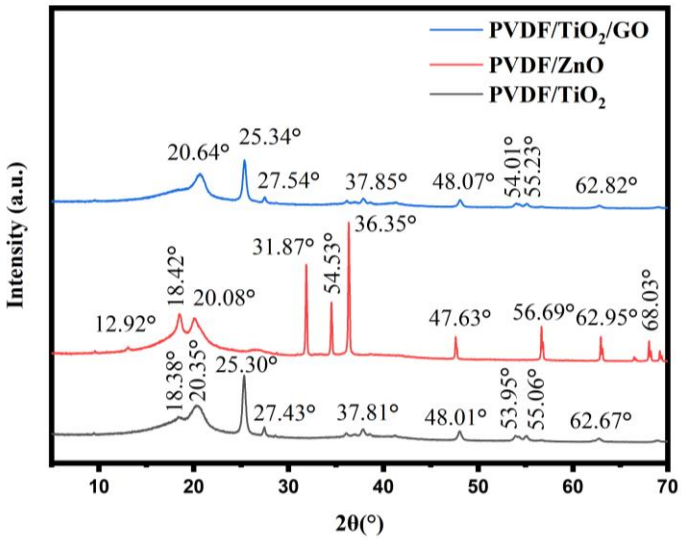

Figure 6. displays XRD patterns of the fabricated PVDF-based nanocomposite photocatalyst membranes.

Adsorption-photocatalysis performance

The adsorption-photocatalytic performance of the PVDF-based nanocomposite photocatalyst membranes is summarized in Table 2. According to the data, the PVDF/ZnO membrane exhibited a lower adsorption-photocatalytic efficiency (89.80%) compared to the PVDF/TiO_2 membrane (91.38%). This disparity can be attributed to the elevated band gap energy in ZnO, leading to an increased recombination rate of electrons and holes. Consequently, the material's capacity to absorb a limited range of UV light is compromised, impacting its overall performance [33].

Upon the incorporation of graphene oxide (GO), the PVDF/TiO_2/GO membranes exhibited a superior MB degradation percentage (91.89%) compared to both PVDF/TiO_2 and PVDF/ZnO membranes. This enhancement is ascribed to the exceptional electron transport properties of GO, acting as an electron acceptor and prolonging the lifetime of charge carriers during the MB degradation process [10]. Consequently, the utilization of GO effectively mitigates the electron-hole recombination issue commonly encountered in metal oxide-based composites, thereby enhancing the overall degradation efficiency.

Moreover, the PVDF/TiO_2/GO membrane undergoes an increase in the generation of ROS when exposed to UV light compared to PVDF/TiO_2 and PVDF/ZnO membrane. This event exhibits a significant and efficient impact on the degradation of the MB dye. The complex interaction among the photocatalytic material, UV light, and the resulting production of ROS highlights the dynamic aspect of the photocatalytic process. The differences in adsorption-photocatalytic efficiency between the PVDF-based nanocomposite photocatalyst membranes provide insights into the factors that affect their performance. These differences highlight the importance of band gap energy and ROS generation in determining the overall effectiveness of these nanocomposite photocatalyst membranes.

Table 2. provides a comprehensive overview of the adsorption-photocatalytic performance of the fabricated PVDF-based nanocomposite photocatalyst membranes, measured over a 24-hour period.

Membranes	PVDF/TiO_2	PVDF/ZnO	PVDF/TiO_2/GO
MB dye degradation percentages (%)	91.38	89.80	91.89

CONCLUSION

In conclusion, a series of PVDF-based nanocomposite photocatalyst membranes were successfully fabricated using the NIPS method. The assessment of MB dye degradation efficiency revealed that the PVDF/TiO_2/GO membrane exhibited the highest performance at 91.89%, surpassing both PVDF/TiO_2

(91.36%) and PVDF/ZnO (89.80%). The incorporation of GO is believed to have significantly contributed to the enhanced degradation efficiency in the PVDF/TiO_2/GO composite. The abundant oxygen-containing functional groups in GO acted as effective electron traps, capturing electrons generated by light and minimizing their recombination with holes. This mechanism ultimately promoted more efficient charge separation.

Furthermore, the PVDF/TiO_2/GO membrane demonstrated a larger pore size compared to its counterparts, PVDF/TiO_2 and PVDF/ZnO. This larger pore size not only facilitated the adsorption of MB but also reduced pore obstruction, facilitating the movement of substances. In essence, the PVDF/TiO_2/GO membranes exhibit promising potential for application as photocatalyst membranes in the adsorption-photocatalysis process for the treatment of dye contamination. The synergistic effects of GO in enhancing degradation efficiency and optimizing pore characteristics make these membranes a noteworthy candidate for further exploration in environmental remediation applications.

DECLARATION OF INTEREST

The authors confirm that there is no conflict of interest.

ACKNOWLEDGEMENT

The authors express gratitude for the financial support received from the Fundamental Research Grant Scheme (grant no. 2020-0254-103-02) and International Grant Kementerian Agama Republik Indonesia (Grant No. 2023-0029-103-11).

REFERENCES

[1] S. M. Anisuzzaman, C. G. Joseph, C. K. Pang, N. A. Affandi, S. N. Maruja, and V. Vijayan, "Current Trends in the Utilization of Photolysis and Photocatalysis Treatment Processes for the Remediation of Dye Wastewater: A Short Review," *ChemEngineering*, vol. 6, no. 4, 2022, doi: 10.3390/chemengineering6040058.

[2] C. Zhou, Y. Sun, F. Zhang, and Y. Wu, "Degradation of minocycline by the adsorption–catalysis multifunctional PVDF–PVP–TiO2 membrane: Degradation kinetics, photocatalytic efficiency, and toxicity of products," *Int. J. Environ. Res. Public Health*, vol. 18, no. 23, 2021, doi: 10.3390/ijerph182312339.

[3] R. Farouq, "Coupling Adsorption-Photocatalytic Degradation of Methylene Blue and Maxilon Red," *J. Fluoresc.*, vol. 32, no. 4, pp. 1381–1388, 2022, doi: 10.1007/s10895-022-02934-1.

[4] A. Popa *et al.*, "Tailoring the RhB removal rate by modifying the PVDF membrane surface through ZnO particles deposition," *J. Inorg. Organomet. Polym. Mater.*, vol. 31, no. 4, pp. 1642–1652, 2021, doi: 10.1007/s10904-020-01795-0.

[5] A. Rabadanova *et al.*, "Piezo-, photo- and piezophotocatalytic activity of electrospun fibrous PVDF/CTAB membrane," *Chim. Techno Acta*, vol. 9, no. 4, pp. 4–11, 2022, doi: 10.15826/chimtech.2022.9.4.20.

[6] M. Sboui, W. Niu, G. Lu, K. Zhang, and J. H. Pan, "Electrically conductive TiO2/CB/PVDF membranes for synchronous cross-flow filtration and solar photoelectrocatalysis," *Chemosphere*, vol. 310, no. July 2022, p. 136753, 2023, doi: 10.1016/j.chemosphere.2022.136753.

[7] J. Chen, J. Wei, H. Zhang, X. Wang, L. Fu, and T.-H. Yang, "Construction of CuCd-BMOF/GO composites based on phosphonate and their boosted visible-light photocatalytic degradation," *Appl. Surf. Sci.*, vol. 594, 2022, doi: 10.1016/j.apsusc.2022.153493.

[8] R. Mohamat *et al.*, "Effect of triple-tail surfactant on the morphological properties of polyethersulfone-based membrane and its antifouling ability," *J. Mater. Sci.*, vol. 57, no. 34, pp. 16333–16351, 2022, doi: 10.1007/s10853-022-07646-2.

[9] M. A. Abu-Dalo, S. A. Al-Rosan, and B. A. Albiss, "Photocatalytic degradation of methylene blue using polymeric membranes based on cellulose acetate impregnated with zno nanostructures," *Polymers (Basel).*, vol. 13, no. 19, 2021, doi: 10.3390/polym13193451.

[10] D. Zhang, F. Dai, P. Zhang, Z. An, Y. Zhao, and L. Chen, "The photodegradation of methylene blue in water with PVDF/GO/ZnO composite membrane," *Mater. Sci. Eng. C*, vol. 96, no. March 2018, pp. 684–692, 2019, doi: 10.1016/j.msec.2018.11.049.

[11] R. Mohamat *et al.*, "Methylene blue rejection and antifouling properties of different carbonaceous additives-based polyvinylidene fluoride membrane," *Mater. Today Commun.*, vol. 35, 2023, doi: 10.1016/j.mtcomm.2023.105862.

[12] S. Sheshmani and M. Nayebi, "Modification of TiO 2 with graphene oxide and reduced graphene oxide; enhancing photocatalytic activity of TiO 2 for removal of remazol Black B," *Polym. Compos.*, vol. 40, no. 1, pp. 210–216, 2019, doi: 10.1002/pc.24630.

[13] Y. Chen, Z. Xiang, D. Wang, J. Kang, and H. Qi, "Effective photocatalytic degradation and physical adsorption of methylene blue using cellulose/GO/TiO2hydrogels," *RSC Adv.*, vol. 10, no. 40, pp. 23936–23943, 2020, doi: 10.1039/d0ra04509h.

[14] Puneetha, N. Kottam, and R. A, "Investigation of photocatalytic degradation of crystal violet and its correlation with bandgap in ZnO and ZnO/GO nanohybrid," *Inorg. Chem. Commun.*, vol. 125, no. November 2020, p. 108460, 2021, doi: 10.1016/j.inoche.2021.108460.

[15] K. Fischer, M. Grimm, J. Meyers, C. Dietrich, R. Gläser, and A. Schulze, "Photoactive microfiltration membranes via directed synthesis of TiO2 nanoparticles on the polymer surface for removal of drugs from water," *J. Memb. Sci.*, vol. 478, pp. 49–57, 2015, doi: 10.1016/j.memsci.2015.01.009.

[16] R. Mohamat *et al.*, "Incorporation of Different Polymeric Additives for Polyvinylidene Fluoride Membrane Fabrication and Its Performance on Methylene Blue Rejection and Antifouling Improvement," *J. Polym. Environ.*, no. 0123456789, 2023, doi: 10.1007/s10924-023-02774-5.

[17] R. Mohamat *et al.*, "Incorporation of graphene oxide/titanium dioxide with different polymer materials and its effects on methylene blue dye rejection and antifouling ability," *Environ. Sci. Pollut. Res.*, vol. 30, no. 28, pp. 72446–72462, 2023, doi: 10.1007/s11356-023-27207-7.

[18] O. Benhabiles, F. Galiano, T. Marino, H. Mahmoudi, H. Lounici, and A. Figoli, "Preparation and characterization of TiO2-PVDF/PMMA blend membranes using an alternative non-toxic solvent for UF/MF and photocatalytic application," *Molecules*, vol. 24, no. 4, pp. 1–20, 2019, doi: 10.3390/molecules24040724.

[19] Z. Warren, T. Tasso Guaraldo, A. S. Martins, J. Wenk, and D. Mattia, "Photocatalytic foams for water treatment: A systematic review and meta-analysis," *J. Environ. Chem. Eng.*, vol. 11, no. 1, p. 109238, 2023, doi: 10.1016/j.jece.2022.109238.

[20] R. Roshani, F. Ardeshiri, M. Peyravi, and M. Jahanshahi, "Highly permeable PVDF membrane with PS/ZnO nanocomposite incorporated for distillation process," *RSC Adv.*, vol. 8, no. 42, pp. 23499–23515, 2018, doi: 10.1039/c8ra02908c.

[21] R. Huang, Y. Dai, J. Ahmed, and M. Edirisinghe, "Facile One-Step Synthesis of PVDF Bead-on-String Fibers by Pressurized Gyration for Reusable Face Masks," *Polymers (Basel).*, vol. 14, no. 21, pp. 1–13, 2022, doi: 10.3390/polym14214498.

[22] E. D. H. Kong *et al.*, "GO/TiO2-Related Nanocomposites as Photocatalysts for Pollutant Removal in Wastewater Treatment," *Nanomaterials*, vol. 12, no. 19, 2022, doi: 10.3390/nano12193536.

[23] M. S. Khan *et al.*, "Graphene quantum dot and iron co-doped TiO2 photocatalysts: Synthesis, performance evaluation and phytotoxicity studies," *Ecotoxicol. Environ. Saf.*, vol. 226, p. 112855, 2021, doi: 10.1016/j.ecoenv.2021.112855.

[24] H. Zhang *et al.*, "Synthesis and characterization of TiO2/graphene oxide nanocomposites for photoreduction of heavy metal ions in reverse osmosis concentrate," *RSC Adv.*, vol. 8, no. 60, pp. 34241–34251, 2018, doi: 10.1039/c8ra06681g.

[25] A. Nasir, S. Khalid, T. Yasin, and A. Mazare, "A Review on the Progress and Future of TiO2/Graphene Photocatalysts," *Energies*, vol. 15, no. 17, pp. 1–34, 2022, doi: 10.3390/en15176248.

[26] M. Jarvin, S. A. Kumar, G. Vinodhkumar, E. Manikandan, and S. S. R. Inbanathan, "Enhanced photocatalytic performance of Hausmannite Mn3O4-rGO nanocomposite in degrading methylene blue," *Mater. Lett.*, vol. 305, no. September, p. 130750, 2021, doi: 10.1016/j.matlet.2021.130750.

[27] M. Abdelmaksoud, A. Mohamed, A. Sayed, and S. Khairy, "Physical properties of PVDF-GO/black-TiO2 nanofibers and its photocatalytic degradation of methylene blue and malachite green dyes," *Environ. Sci. Pollut. Res.*, vol. 28, no. 24, pp. 30613–30625, 2021, doi: 10.1007/s11356-021-12618-1.

[28] P. Pascariu *et al.*, "Graphene and TiO 2 - PVDF Nanocomposites for Potential Applications in Triboelectronics," *Proc. Int. Semicond. Conf. CAS*, vol. 2018-Octob, pp. 237–240, 2018, doi: 10.1109/SMICND.2018.8539781.

[29] J. D. Rosario *et al.*, "Synergistic effect of impure/pure graphene oxide and TiO2 fillers on the dielectric properties of poly (vinylidene fluoride- hexafluoropropylene) for electroadhesive high load bearing applications," *J. Electroceramics*, vol. 50, no. 1, pp. 23–36, 2023, doi: 10.1007/s10832-022-00301-x.

[30] M. Cantarella *et al.*, "Selective photodegradation of paracetamol by molecularly imprinted ZnO nanonuts," *Appl. Catal. B Environ.*, vol. 238, pp. 509–517, 2018, doi: 10.1016/j.apcatb.2018.07.055.

[31] M. A. Hanif *et al.*, "Enhanced photocatalytic and antibacterial performance of ZnO nanoparticles prepared by an efficient thermolysis method," *Catalysts*, vol. 9, no. 7, 2019, doi: 10.3390/catal9070608.

[32] M. Najafi, A. Kermanpur, M. R. Rahimipour, and A. Najafizadeh, "Effect of TiO2 morphology on structure of TiO2-graphene oxide nanocomposite synthesized via a one-step hydrothermal method," *J. Alloys Compd.*, vol. 722, pp. 272–277, 2017, doi: 10.1016/j.jallcom.2017.06.001.

[33] H. S. Zakria, M. H. D. Othman, R. Kamaludin, S. H. Sheikh Abdul Kadir, T. A. Kurniawan, and A. Jilani, "Immobilization techniques of a photocatalyst into and onto a polymer membrane for photocatalytic activity," *RSC Adv.*, vol. 11, no. 12, pp. 6985–7014, 2021, doi: 10.1039/d0ra10964a.